Progress In Electromagnetics Research C, Vol. 78, 47–55, 2017

Wideband Omnidirectional Circularly Polarized Patch Antenna with Multi-Resonant Structure

Long Yang[1, *], Zhi-Ya Zhang[1], Luyang Ji[2], Dan Wu[1], Guang Fu[1], and Zehong Yan[1]

Abstract—A wideband omnidirectional circularly polarized (CP) patch antenna is proposed in this paper. The proposed antenna is composed of a disk-loaded coaxial probe and four pairs of modified Γ-shaped strips loaded with shorting pins. Each pair of modified Γ-shaped strips consists of an inner Γ-shaped strip and an outer Γ-shaped strip. The approach employed in this design for improving the operating bandwidth is to add an inner Γ-shaped strip and make it couple to the outer one. By introducing the two coupled Γ-shaped strips, two different monopole modes can be achieved simultaneously and controlled separately by two different corresponding parts of these two Γ-shaped strips, respectively, and they can be merged to realize a wide-band impedance matching. Meanwhile, two minimum axial ratio (AR) points around the resonances of the antenna are excited by the coupled Γ-shaped strips, and they can be reallocated closely to each other for wide AR bandwidth. The measured results show that the proposed design has a 10-dB impedance bandwidth of 22.7% (2.26–2.84 GHz), 3-dB AR bandwidth of 33.6% (2.1–2.95 GHz) and low profile of $0.1\lambda_0$ (λ_0 is the free-space wavelength at center frequency). In addition, a parametric discussion is conducted to further verify the proposed design.

1. INTRODUCTION

Omnidirectional CP antennas are relatively insensitive to their respective orientations when transmitting and receiving signals. Also, they can suppress the multi-path effects caused by nearby circumstance [1–3]. Thus, the omnidirectional CP antennas are good candidates for various wireless systems [4].

Omnidirectional CP antenna is usually achieved by exciting two orthogonal polarized fields of equal amplitude but in phase quadrature just by a single feeding line [5–7]. Typically, a vertically polarized field against the ground can be generated by monopole-like antennas. Later, based on the metamaterial transmission line (MTL), a zeroth-order resonance (ZOR) antenna is proposed to generate vertically polarized field [8]. A horizontally polarized field can be obtained by a magnetic dipole, which is realized by an Alford loop antenna and its derivatives [9, 10]. Generally, omnidirectional CP radiation is obtained by an appropriate combination of the two structures mentioned above. In [11], a low-profile omnidirectional CP antenna is proposed which consists of a top-loaded cylindrical monopole and four printed arc-shaped dipoles. In [12], the presented antenna uses a monopole and a loop radiator to achieve omnidirectional CP property. Based on the ZOR of the MTL and curved branches, a novel omnidirectional CP antenna is reported in [13]. Though the single-fed CP antennas in [11–13] are in low profile, they typically have narrow 10-dB impedance bandwidths (less than 14%). Additionally, dual-band omnidirectional CP antennas are investigated either by using the ZOR and FOR modes of

Received 13 July 2017, Accepted 14 September 2017, Scheduled 21 September 2017

* Corresponding author: Long Yang (wuyanqianzi@163.com).

[1] Science and Technology On Antenna and Microwave Laboratory, Collaborative Innovation Center of Information Sensing and Understanding, Xidian University, Xi'an, 710071 China. [2] School of Electronics and Information, Northwestern Polytechnical University, Xi'an 710000, China.

the MTL [14] or by using the TM_{01} and TM_{02} modes of the microstrip antenna [15]. However, their narrow operating bandwidth is still a challenge for future applications.

Several techniques have been proposed to broaden the impedance bandwidth of the single-fed omnidirectional CP antenna. One method is to utilize symmetrical wideband radiation elements. A wideband omnidirectional CP antenna employs four broadband rectangular loop elements which are symmetrically located on the surface of a hollow dielectric cylinder [16]. Its 10-dB impedance bandwidth is 41% with a 3-dB AR bandwidth of 45%. However, this antenna requires a complicated network, consisting of wideband balun and impedance matching circuits. Another approach is to introduce a dielectric resonance antenna (DRA). Loaded by some parasitic metallic strips, the DRA in [17] achieves a wide overlapped 10-dB impedance and 3-dB AR bandwidth of about 25%. Though the DRA has a simple structure and wide bandwidth, its profile is relatively high. Recently, a new method has been presented, which is realized by combining two different modes or more to achieve a wider bandwidth. In [18], by employing vortex slots and shorting vias on a microstrip antenna, three resonant modes are excited, and these modes can be coupled together to obtain a bandwidth of more than 50%. However, the design has a drawback: its maximum radiation directions are not at the horizontal plane ($\theta = 90^\circ$). In [19], by using two groups of slots both on the patch and the ground, a wide impedance bandwidth about 22% is obtained with two resonances. In [20], by loading vias on the patch, the TM_{01} mode is generated and coupled to the TM_{02} mode, and a wide bandwidth about 16.6% is achieved. However, their AR bandwidths in [19, 20] are not wide enough to cover their impedance bandwidths.

This paper presents a wideband omnidirectional CP antenna with two different resonances of the monopole mode. The antenna consists of a square patch fed by coaxial probe and modified Γ-shaped strips with shorting pins. Though the antennas in [11–13] use a similar configuration, they provide only a narrow bandwidth since just one resonance is excited. In this paper, a multi-resonant structure is adopted by adding an inner Γ-shaped strip inside the outer one, and as a result, the proposed antenna achieves another resonance of the monopole mode and provides a wide bandwidth. One advantage of the design is that two resonances can be achieved separately by the two different Γ-shaped strips. Meanwhile, they can also be controlled simultaneously by these two Γ-shaped strips, which makes the impedance matching convenient and accelerates the design process. Another advantage of the design is that two minimum AR points occur around the two resonances, thus its 3-dB axial ratio bandwidth can be greatly improved. The measured results show that the proposed design has two adjacent resonances and provides a 10-dB impedance bandwidth of 22.7% (2.26–2.84 GHz) and a 3-dB AR bandwidth of 33.6% (2.1–2.95 GHz). Moreover, the antenna exhibits a good omnidirectional left-handed CP radiation, and it has a structure with a dimension of $0.55\lambda_0 \times 0.55\lambda_0 \times 0.1\lambda_0$.

2. ANTENNA DESIGN AND DISCUSSION

Figure 1 shows the configuration of the proposed antenna. It consists of a ground plane and a radiator which are both printed on a 1 mm-thick substrate ($\varepsilon_r = 2.65$, $\tan\delta = 0.002$), with a radius of 35 mm. The radiator is composed of a square patch in the middle and four unit cells, as shown in Fig. 1(b). Each unit cell employs an outer Γ-shaped strip outside and an inner Γ-shaped strip with shorting pin inside, as shown in Fig. 1(c). The outer Γ-shaped strip has an arc length of L_0 and width of Wa, while the inner Γ-shaped strip has an arc length of 40 mm and width of Wb. The distance of the curved parts between the two Γ-shaped strips is gap_0, while the distance of the straight parts is gap_2. Gap_1 is introduced between the two adjacent units to widen the bandwidth. The proposed antenna is fed by a conducting pin with a height of h_0 and radius of 1.5 mm in the center of the square patch for achieving symmetrical radiation pattern. The detailed parameters of this design are listed: $gap_0 = 1.0$ mm, $gap_1 = 3$ mm, $gap_2 = 3.5$ mm, $L_0 = 30$ mm, $Wa = 3$ mm, $Wb = 6$ mm, $W_1 = 14$ mm, $W_2 = 0.7$ mm, $W_3 = 4$ mm, $P = 11$ mm, $R_0 = 32$ mm, $Rg = 30$ mm, $h_0 = 12$ mm.

In this design, the monopole mode is excited by the patch and Γ-shaped strips with shorting pins. An inner Γ-shaped strip is introduced inside the outer Γ-shaped strip in each unit cell, which can generate another resonance of the monopole mode, leading to a wider bandwidth. To better illustrate the wideband operating principle, the magnetic field on the patch and the surface current distribution of one unit are shown in Fig. 2. It can be seen from Fig. 2(a) that the direction of the current on the coaxial probe points to $+z$ direction due to the magnetic fields around the probe in the counter-

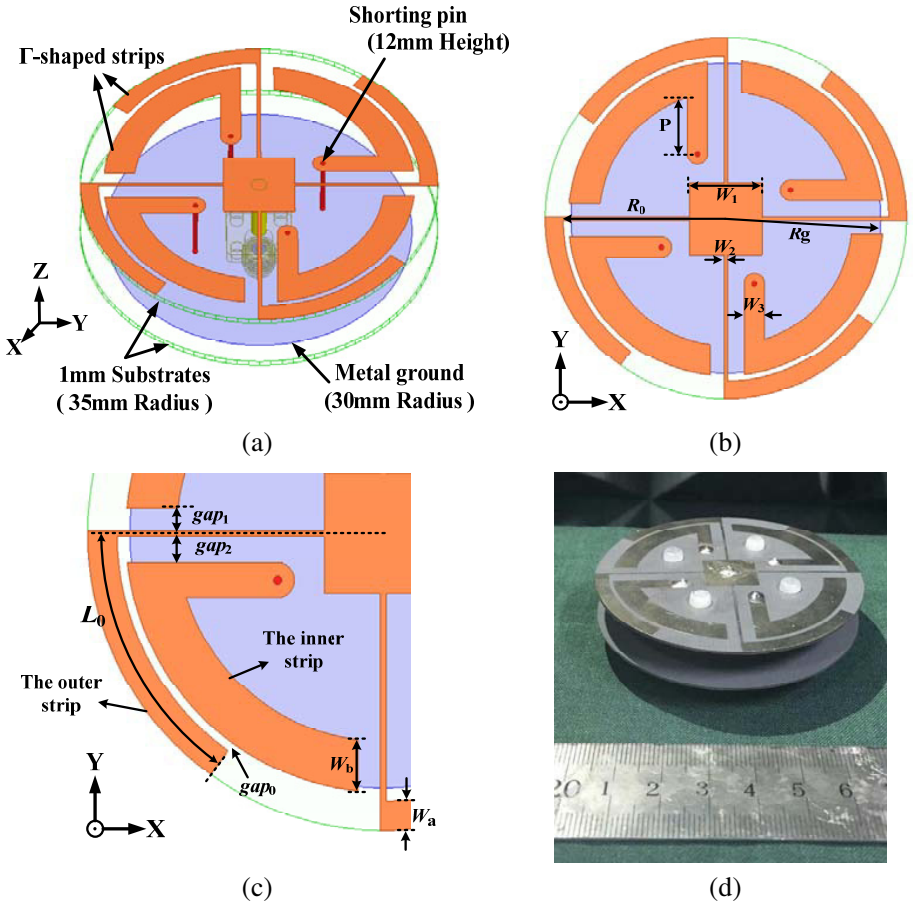

Figure 1. Configuration of the proposed design. (a) 3-D view. (b) Top view. (c) Unit cell. (d) Photograph of the prototype.

clockwise direction (according to the boundary condition $\vec{J} = \vec{n} \times \vec{H}$), which dominates the E_θ field, thus the low-frequency mode of the monopole mode is achieved. The E_φ field is dominated by the current in the φ direction flowing along the outer strip as shown in Fig. 2(d). The current flows from the outer Γ-shaped strip to the shorting pin then to the ground. From Figs. 2(b) and (e), it is seen that the high-frequency mode of the monopole mode is generated. The current flows from the square patch to the inner Γ-shaped strip then to the ground, indicating that another current path is formed which is different from that of the low-frequency mode. However, in this case, E_θ field is generated by the shorting pins because the magnetic field around it is growing stronger than that around the probe, and E_φ is dominated by the current in the φ direction flowing along the inner strip as shown in Fig. 2(e). Therefore, the two resonances are generated by different curved branches, and they can be coupled to each other to achieve a wide impedance bandwidth when the parameters relevant to the two curved strips are appropriately selected.

In the design, the monopole mode of the patch antenna is excited by the disk-loaded coaxial probe for generating the E_θ field, and the Γ-shaped strips are utilized to achieve the E_φ field. Omnidirectional CP radiation pattern is obtained once the two orthogonal fields are equal in amplitude but in phase quadrature [18, 21, 22]. The E_θ and E_φ fields can be expressed as:

$$\begin{cases} \vec{E}_\theta = j\dfrac{I_d L_d \omega \mu_0}{4\pi r} \sin\theta \cdot \hat{\theta} \\ \vec{E}_\varphi = \dfrac{I_l a \omega \mu_0}{2r} J_1(\beta a \sin\theta) \cdot \hat{\varphi} \end{cases} \tag{1}$$

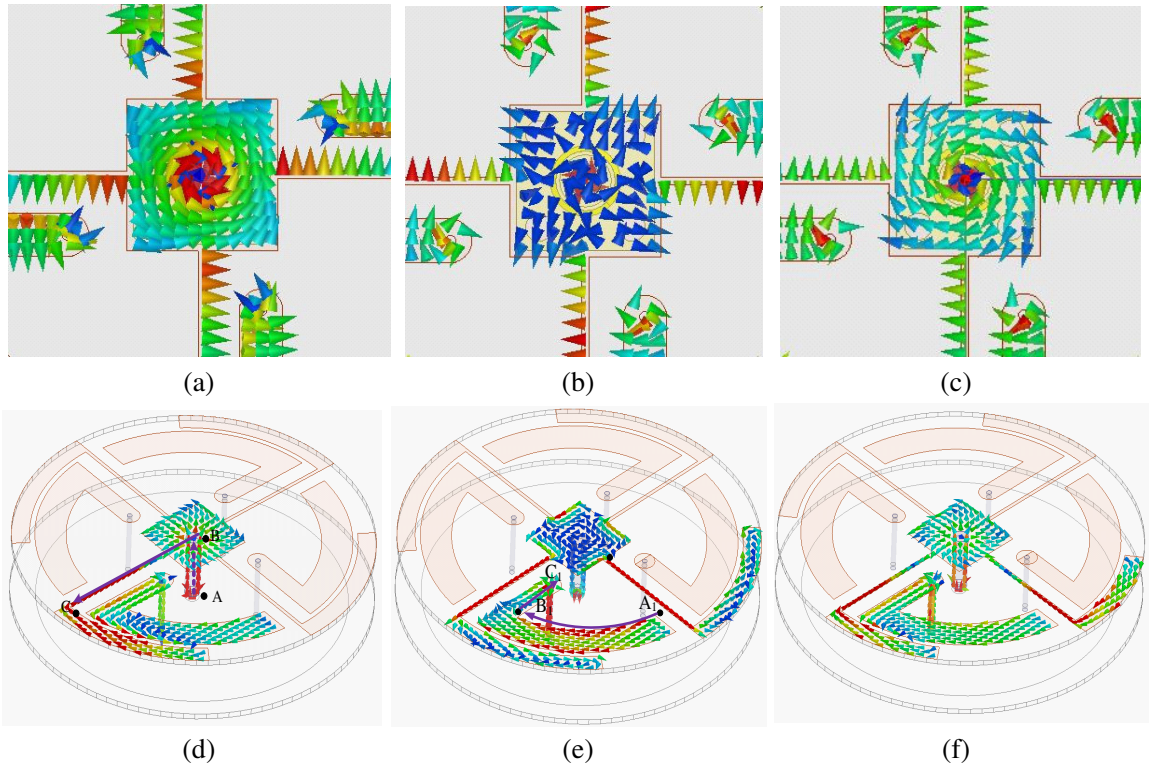

Figure 2. Magnetic field (up) on the patch and surface current distribution (down) of the unit. (a) (d) low-frequency mode (2.35 GHz). (b) (e) high-frequency mode (2.75 GHz). (c) (f) hybrid mode at 2.55 GHz when L_0 equals to 20 mm.

where I_d and I_l are the currents on the probe or the shorting pins and the curved strips, respectively. L_d is the length of the probe or the shorting pins, a the radius of the current loop, ω the frequency, μ_0 the permeability, r the distance from the antenna, and J_1 the first-order Bessel function. The imaginary number j in Eq. (1) indicates that the two components have 90° delayed phase difference intrinsically when the probe or the shorting pins and the current loop are simultaneously excited in phase. This, of course, only applies to the condition that the current loop is small enough. Here, for the large current loop, the path difference $\Delta\theta$ between the probe or the shorting pins and the current loop should meet the constraint condition: $\Delta\theta = \pm n\pi$. For the low-frequency mode, seen from Fig. 2(d), the distance between the probe and the current loop is denoted by the purple line, and the path difference is $\Delta\theta_1 \approx \beta \cdot (AB + BC) \approx \pi$, which can meet the constraint condition. For the high-frequency mode, seen from Fig. 2(e), the path difference is $\Delta\theta_2 \approx \beta \cdot (A_1B_1 + B_1C_1) \approx 1.1\pi$, which can also meet the constraint condition. For the low-frequency mode, the delayed phase depends on the radius of the current loop (R_0) and height (h_0) of the antenna. On the other hand, for the high-frequency mode, it mainly depends on R_0 and the location of the shorting pins (p). Thus, the dimensions of the corresponding structure should meet the constraint condition for a good CP performance when designing the antenna.

It is noted that two minimum AR points occur around the two resonances, thus wide 3-dB axial ratio bandwidth is achieved. Since the curved strips are located symmetrically around the center and have the same field distribution, the proposed antenna can realize an omnidirectional CP radiation pattern in the azimuth plane. The direction of the CP field is determined by the rotary direction of the Γ-shaped strips. Therefore, the proposed antenna radiates a left-hand (LH) CP wave due to the counterclockwise arrangement of the Γ-shaped strips. Conversely, the right-hand (RH) CP radiation can be achieved when the Γ-shaped strips are arranged clockwise.

3. PARAMETER DISCUSSION

To demonstrate the operating principle of the proposed antenna, a parameter study has been conducted among L_0, gap_1, gap_2, P and Rg to show their effects on the S_{11} and the AR at $\Phi = 0°$, $\theta = 90°$ by using HFSS 15. In the parametric discussion, all the other parameters are fixed.

Figure 3 shows the simulated S_{11} and AR bandwidths with different lengths of the outer Γ-shaped strip ($L_0 = 20$, 25, 30 and 35 mm). It is shown that L_0 has significant effects on the bandwidths of the proposed antenna: the resonant frequency and the minimum AR point of the low-frequency mode shift upward as L_0 decreases, while the resonant frequency and the minimum AR point of the high-frequency mode are insensitive to the variation of L_0. This verifies that the low-frequency mode is controlled by the outer Γ-shaped strip. It is noted that a hybrid mode is obtained since the two modes merge into one when L_0 decreases to 20 mm. The magnetic field and current distributions of the hybrid mode at 2.55 GHz are shown in Fig. 2(c) and Fig. 2(f), respectively, when L_0 equals 20 mm. In this case, it is seen that both low-frequency and high-frequency modes exist, providing two different resonant modes. The variation of AR is the same as that of S_{11}, indicating that the matching of the low-frequency mode and the values of AR in the low frequency band can be tuned simultaneously by L_0.

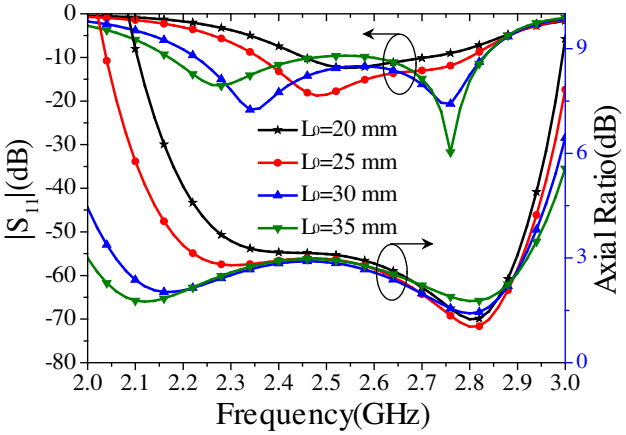

Figure 3. Simulated reflection coefficient and AR of the design for different lengths of the outer Γ-shaped strip.

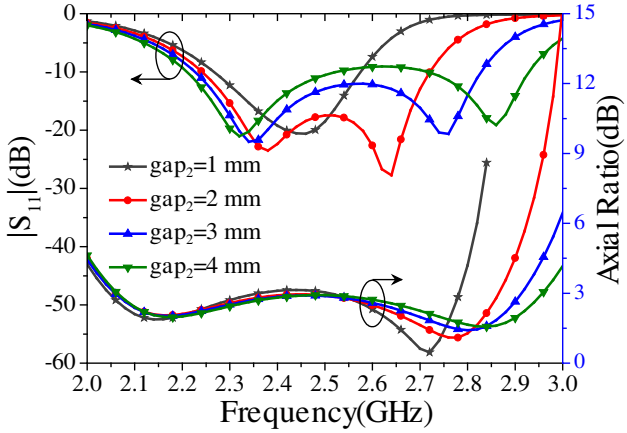

Figure 4. Simulated reflection coefficient and AR of the design for gap_2.

Figure 4 also shows the effects of gap_2 on the S_{11} and AR. As shown in Fig. 4, the impedance matching of the upper band is significantly affected by gap_2. The resonant frequency of the high-frequency mode decreases dramatically from 2.85 GHz to 2.45 GHz when gap_2 decreases from 4 to 1 mm, while the resonant frequency for the low-frequency mode remains almost unchanged. The minimum AR points for both the modes change similarly as S_{11} does. It is expected because the length of the inner Γ-shaped strip becomes longer while the outer Γ-shaped strip is unchanged as gap_2 decreases. The results of S_{11} with different values of gap_2 show that the high-frequency mode is introduced by the inner Γ-shaped strip, and the two modes can operate independently. Thus, the matching of the two resonances can be tuned separately, while the AR and S_{11} can be tuned simultaneously, which is of great value for simplifying the design. The effects of the location of the shorting pins (p) are shown in Fig. 5. The results show that the resonant frequencies of the two modes both shift downwards as P increases. This is expected because both the current paths of the two modes become larger as P increases. The minimum AR point for the high-frequency mode is more sensitive than the lower one since a more delayed phase between E_θ and E_φ is obtained when it works at the high-frequency mode.

The effects of the gap between two adjacent units are also discussed. The simulated S_{11}s and ARs with different gap_1 values (1.5, 2, and 3 mm) are depicted in Fig. 6. Another resonance occurs at the upper band as gap_1 increases. This is because a larger gap between the two adjacent units leads to a weaker coupling, which affects the field distributions of both the modes slightly. The AR bandwidth

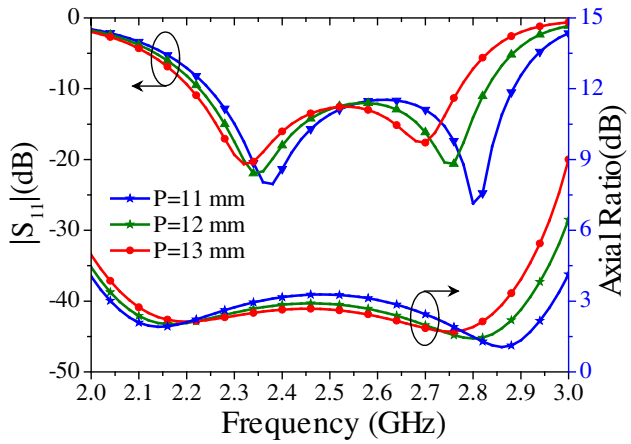

Figure 5. Simulated reflection coefficient and AR of the design for different positions of the shorting pin.

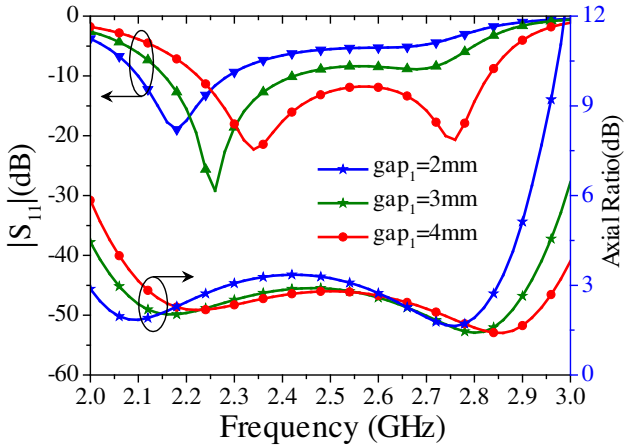

Figure 6. Simulated reflection coefficient and AR for different gaps between two adjacent units.

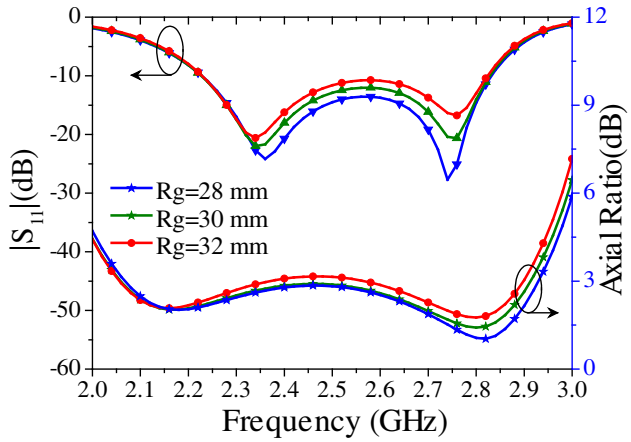

Figure 7. Simulated reflection coefficient and AR of the design for different size of the ground.

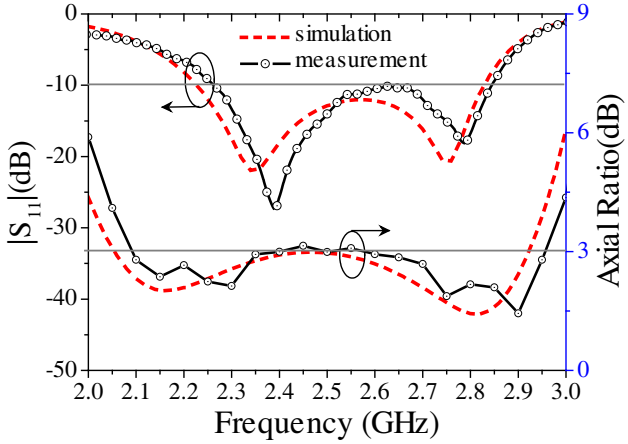

Figure 8. Measured and simulated reflection coefficient and AR.

shifts downward, and the AR in the middle band deteriorates as gap_1 decreases. Thus, the gap between the two adjacent units should be appropriately chosen in order to achieve a wideband performance.

Figure 7 shows the simulated S_{11}s and ARs with different sizes of the ground plane (Rg = 28, 30, and 32 mm). When Rg decreases, the impedance matching in the operating band improves with little effects on the resonant frequency and the AR bandwidth. Thus, Rg can be used to tune the impedance matching after a good AR is obtained.

In summary, the dimensions of the outer and inner Γ-shaped strips can deeply affect the characteristics of the proposed antenna. Moreover, the outer and inner Γ-shaped strips can be utilized to tune the performances, namely the resonant frequencies and minimum AR points of the proposed antenna at low-frequency and high-frequency modes, respectively.

4. EXPERIMENTAL RESULTS

A prototype is fabricated and measured. Fig. 1(d) shows a photograph of the prototype. The measurements are carried out using Agilent E8363B network analyzer and an anechoic chamber. Fig. 8 shows the simulated and measured reflection coefficients and ARs against the frequency for the proposed antenna. The measured 10-dB impedance bandwidth is about 22.7% (2.26–2.84 GHz) which is narrower

than the simulated results about 23.7% (2.23–2.83 GHz). The AR results are measured when $\Phi = 0°$, $\theta = 90°$. The simulated and measured 3-dB AR bandwidths are 36% (2.05–2.95 GHz) and 33.6% (2.1–2.95 GHz), respectively. Measured results agree well with the simulated ones. The two resonances shift upwards slightly. The discrepancy is caused by the manufacturing tolerance. The AR bandwidth is wider than the impedance bandwidth, which indicates that the proposed antenna can realize a good CP radiation within a wide operating frequency band.

Figure 9 shows the simulated and measured far-field radiation patterns in the elevation ($\Phi = 0°$) and azimuth ($\theta = 90°$) planes at the two modes. The patterns of the azimuth and elevation planes are both monopole-like. Compared to the traditional monopoles, the proposed antenna can radiate CP waves. The differences between the LHCP and RHCP gains are more than 15 dB at the directions of $\Phi = 0°$, $\theta = 90°$ for the two modes. Due to the symmetry of the structure, the measured gain variations are less than 1 dB in the azimuth plane ($\theta = 90°$) for the two modes, which indicates that the proposed antenna can realize an excellent omnidirectional radiation performance.

The measured ARs at the two modes in the azimuth plane are given in Fig. 10. It is seen that the ARs of the proposed antenna are low (lower than 3.3 dB and 2.5 dB for low-frequency mode and high-frequency mode, respectively) with the ripples less than 1 dB for both modes. Fig. 11 shows the simulated and measured antenna gains and simulated radiation efficiency versus frequency at $\Phi = 0°$, $\theta = 90°$. A reasonable agreement between simulated and measured antenna gains is obtained. It is seen that the measured average LHCP gain is around 1.0 dBic and 0 dBic at the lower band and upper band, respectively. In addition, the radiation efficiency is above 90% in the whole operating bandwidth.

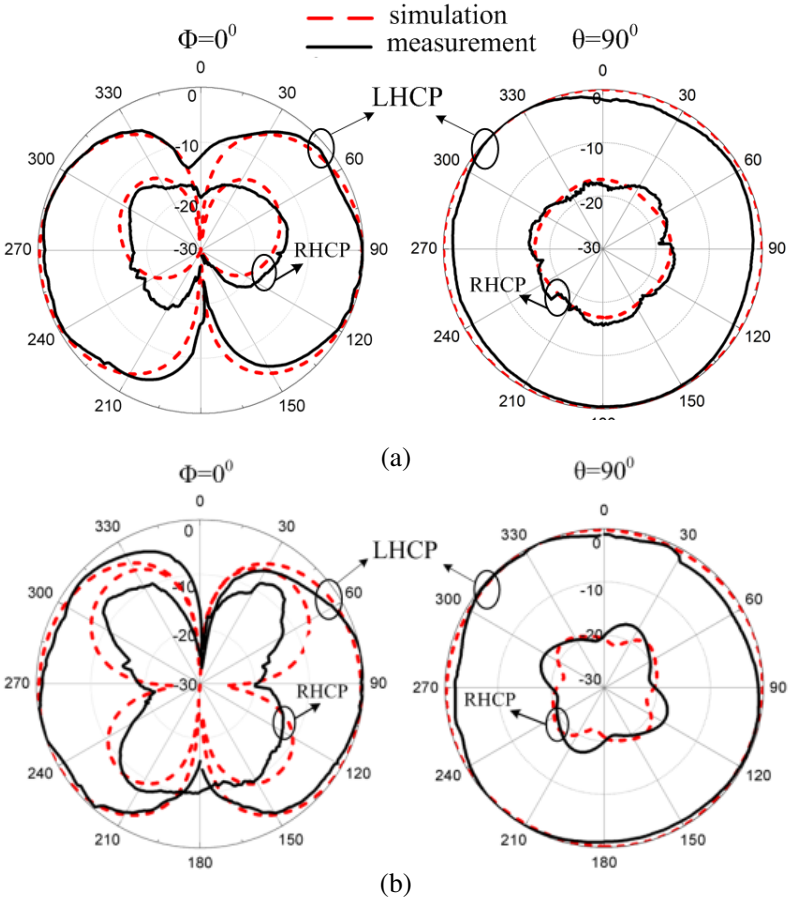

Figure 9. Simulated and measured radiation patterns in the elevation ($\Phi = 0°$) (left) and azimuth ($\theta = 90°$) (right) planes. (a) Simulated at 2.35 GHz and measured at 2.4 GHz. (b) Simulated at 2.75 GHz and measured at 2.8 GHz.

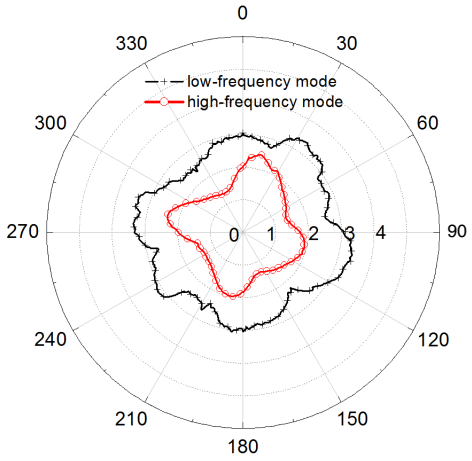

Figure 10. Measured AR at $\theta = 90°$.

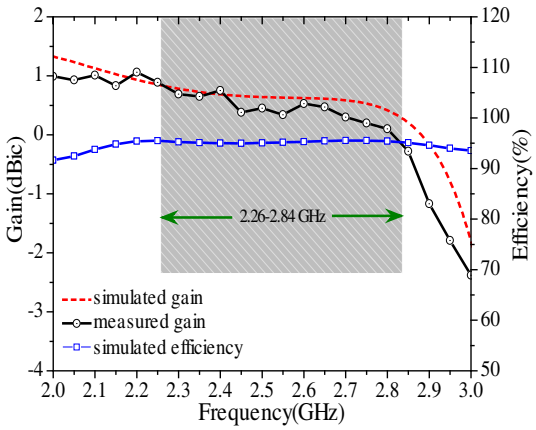

Figure 11. Gains and radiation efficiency (at $\Phi = 0°$, $\theta = 90°$).

5. CONCLUSION

A wideband omnidirectional CP antenna is proposed in this paper based on the monopole mode. By introducing a multi-resonant structure, two resonances are achieved and combined, thus the impedance bandwidth is improved. The operating principle is analyzed in detail by a parameter study. A prototype is fabricated and measured. Measured results show that the AR bandwidth is 33.6% (2.1–2.95 GHz), which can cover the impedance bandwidth of 22.7% (2.26–2.84 GHz). It can be a good candidate for the wireless communication systems due to its advantages of simple structure, wide operating bandwidth, and excellent radiation performances.

ACKNOWLEDGMENT

The authors would like to thank Professor Shuxi Gong and Ying Liu for valuable suggestions. This work was supported by the National Natural Science Foundation of China under Grant No. 61601338 and the Fundamental Research Funds for the Central Universities under Grant JB150507.

REFERENCES

1. Amin, M., J. Yousaf, and S. Iqbal, "Single feed circularly polarised omnidirectional bifilar helix antennas with wide axial ratio beamwidth," *IET Microw. Antennas Propag.*, Vol. 7, No. 10, 825–830, 2013.
2. Sichak, W. and S. Milazzo, "Antennas for circular polarization," *Proceedings of the IRE*, Vol. 36, No. 8, 997–1101, 1948.
3. Chang, T. N. and J. H. Jiang, "Enhance gain and bandwidth of circularly polarized microstrip patch antenna using gap-coupled method," *Progress In Electromagnetics Research*, Vol. 96, 127–139, 2009.
4. Yang, L., N. W. Liu, Z. Y. Zhang, et al., "A novel single feed omnidirectional circularly polarized antenna with wide AR bandwidth," *Progress In Electromagnetics Research C*, Vol. 51, 35–43, 2014.
5. Sharma, P. and K. Gupta, "Analysis and optimized design of single feed circularly polarized microstrip antennas," *IEEE Trans. Antennas Propag.*, Vol. 31, No. 6, 949–955, 1983.
6. Iwasaki, H., "A circularly polarized rectangular microstrip antenna using single-fed proximity-coupled method," *IEEE Trans. Antennas Propag.*, Vol. 43, No. 8, 895–897, 1995.
7. Sudha, T., T. S. Vedavathy, and N. Bhat, "Wideband single-fed circularly polarised patch antenna," *Electronics Letters*, Vol. 40, No. 11, 648–649, 2004.

8. Park, J. H., Y. H. Ryu, and J. G. Lee, "Epsilon negative zeroth-order resonator antenna," *IEEE Trans. Antennas Propag.*, Vol. 55, No. 12, 3710–3712, 2007.
9. Wei, K. P., Z. J. Zhang, Z. H. Feng, et al., "A MNG-TL loop antenna array with horizontally polarized omnidirectional patterns," *IEEE Trans. Antennas Propag.*, Vol. 60, No. 6, 2702–2710, 2012.
10. Lin, C. C., L. C. Kuo, and H. R. Chuang, "A horizontally polarized omnidirectional printed antenna for WLAN applications," *IEEE Trans. Antennas Propag.*, Vol. 54, No. 11, 3551–3556, 2006.
11. Wong, K. L. and F. R. Hsiao, "A low-profile omnidirectional circularly polarized antenna for WLAN access point," *Antennas and Propagation Society International Symposium*, 2004.
12. Li, B., S. W. Liao, and Q. Xue, "Omni-directional circularly polarized antenna combining monopole and loop radiators," *IEEE Antennas Wireless Propag. Lett.*, Vol. 12, No. 5, 1102–1105, 2013.
13. Park, B. C. and J. H. Lee, "Omnidirectional circularly polarized antenna utilizing zeroth-order resonance of epsilon negative transmission line," *IEEE Trans. Antennas Propag.*, Vol. 59, No. 7, 2717–2720, 2011.
14. Park, B. C. and J. H. Lee, "Dual-Band omnidirectional circularly polarized antenna using zeroth- and first-order modes," *IEEE Antennas Wireless Propag. Lett.*, Vol. 11, No. 8, 407–410, 2012.
15. Yu, D., S. X. Gong, and Y. T. Wan, "Omnidirectional dual-band dual circularly polarized microstrip antenna using TM_{01} and TM_{02} modes," *IEEE Antennas Wireless Propag. Lett.*, Vol. 13, No. 9, 1104–1107, 2014.
16. Quan, X. L., R. L. Li, and M. M. Tentzeris, "A broadband omnidirectional circularly polarized antenna," *IEEE Trans. Antennas Propag.*, Vol. 61, No. 5, 2363–2370, 2013.
17. Pan, Y. M. and K. W. Leung, "Wideband omnidirectional circularly polarized dielectric resonator antenna with parasitic strips," *IEEE Trans. Antennas Propag.*, Vol. 60, No. 5, 653–659, 2013.
18. Yu, D., S. X. Gong, and Y. T. Wan, "Wideband omnidirectional circularly polarized patch antenna based on vortex slots and shorting vias," *IEEE Trans. Antennas Propag.*, Vol. 62, No. 8, 3970–3977, 2014.
19. Wu, J. J., Z. D. Wang, and Y. Z. Yin, "Wideband omnidirectional circularly polarized antenna with offsetting slots and vertical strips," *International Journal of RF and Microwave Computer-Aided Engineering*, Vol. 25, No. 8, 675–679, 2014.
20. Shi, Y. Z. and J. H. Liu, "Wideband and low-profile omnidirectional circularly polarized antenna with slits and shorting-vias," *IEEE Antennas Wireless Propag. Lett.*, Vol. 15, No. 8, 686–689, 2016.
21. Li, B., S. W. Liao, and Q. Xue, "Omnidirectional circularly polarized antenna combing monopole and loop radiators," *IEEE Antennas Wireless Propag. Lett.*, Vol. 12, 607–610, 2013.
22. Yu, Y. F, Z. X. Shen, and S. L. He, "Compact omnidirectional antenna of circular polarization," *IEEE Antennas Wireless Propag. Lett.*, Vol. 11, 1466–1469, 2012.